

Original Article

# Performance Evaluation of A Hydrodynamic Journal Bearing using Nano Ferro Fluid Lubricants with Varying Concentration of Iron Oxide Nanoparticle Additives ( $\text{Fe}_3\text{O}_4$ )

B. Vijaya Krishna<sup>1</sup>, N. Seetharamaiah<sup>2</sup>, L. Siva Rama Krishna<sup>3</sup>

<sup>1,3</sup>Department of Mechanical Engineering, University College of Engineering, (Osmania University), Telangana, India.

<sup>2</sup>Department of Mechanical Engineering, Gitam School of Technology (Gitam University), Telangana, India.

<sup>1</sup>Corresponding Author : [vjkrishna.mech01@gmail.com](mailto:vjkrishna.mech01@gmail.com)

Received: 13 June 2023

Revised: 24 July 2023

Accepted: 14 August 2023

Published: 31 August 2023

**Abstract** - Hydrodynamic journal bearings are essential for boosting any machine's dependability. When the interplay of geometry, surface motion, and fluid viscosity culminates in generating adequate fluid pressure to uphold the applied load, it gives rise to the formation of a hydrodynamic film. The additional pressure pushes the surfaces apart, preventing them from making contact. This phenomenon is known as hydrodynamic lift. Hydrodynamic lift supports the load on hydrodynamic bearings. Hydrodynamic journal bearings operate within a lubricated environment, where lubrication primarily aims to mitigate friction, wear, and heat generation among machine components undergoing relative motion. Therefore, advancements in lubrication techniques play a pivotal role in profoundly enhancing the effectiveness of these bearings. Modifications to oil lubrication properties are used to monitor bearing behavior. Variations in lubricant properties have a significant impact on how well a bearing works. In the present experimental investigations, the effects of the Nano Ferro Fluid Lubricants. Nano Ferro Lubricants are made by altering the amounts of lubricant additives in concentrations such as 15%, 20%, and 25% in Castrol SAE 30 oil. The viscosity of the lubricating oil increased by adding nanoparticles, which improves the journal bearing's performance characteristics, such as heat absorption and pressure reduction capacity. With the aid of a sophisticated mechanical agitator, nanoparticles utilized for work are combined with base oil in volume fractions of 15%, 20%, and 25%. Experimental research on pressure dissemination, load supporting capacity, bearing characteristic number, friction coefficient, Sommerfeld number, and heat generation is done using a hydrodynamic journal bearing test rig, 500, 600 and 700 rpm are used to assess a bearing's performance along with 100 N, 150 N and 200 N of load. The results show that adding Nano Ferro Particles ( $\text{Fe}_3\text{O}_4$ ) as lubricant additives increases the maximum pressure absorption capacity and load carrying capacity of journal bearings while decreasing bearing characteristic number, coefficient friction, Sommerfeld number, and heat generation when compared to base oil without nanoparticle additives.

**Keywords** - Design parameters, Journal bearing, Lubricant additives, Nano ferro fluids, Volume concentration.

## 1. Introduction

Due to the capacity of a hydrodynamic bearing to support loads based only on fluid pressure when there is no real journal to bearing contact. In rotating machinery, such as huge industrial equipment, Hydrodynamic bearings find widespread use in various applications, including large-scale applications like gearboxes, compressors and pumps, which play vital roles in power generation. [1].

Hydrodynamic journal bearings function by suspending the rotating components on a thin fluid film, commonly known as fluid film bearings. This separation between the moving and

stationary surfaces leads to minimal friction and negligible wear, contributing to the hydrodynamic bearing's remarkably extended lifespan, which can often match the operational life of the machinery. The performance of journal bearings has to be improved. [2] Modern machinery's increasing load and speed conditions present a constant challenge for tribologists as they work to increase the effectiveness and lifespan of the support bearings. In addition to the latest advancements in bearing design, enhancing the oil characteristics is given a lot of emphasis. [3] The technology of the future for the twenty-first century is nanotechnology. Nanoparticles are characterized by their nanometer size and enormous specific surface area.



Nanoparticles are being employed more often to find answers to contemporary technical issues. A brand-new type of lubricant called nano lubricant is created by mixing tiny particles with the basic fluid. Nanofluids have unique characteristics that make them potentially helpful in a wide range of heat transfer applications. Compared to the base fluid, they exhibit enhanced thermal conductivity and convective heat transfer coefficient [4]. Recent research in nanotribology has demonstrated the ability to employ nanoparticles as an addition in lubricant to reduce friction and wear and increase load-bearing capacity. Few investigations have shown that nanofluids have improved rheological behavior compared to base fluids.

Rheological research on nanofluids has become quite important in recent years. Many researchers have investigated the viscosity of water-based nanofluids. Recent findings suggest that these nanofluids often exhibit higher viscosities than non-nano oils. Moreover, the quantity of nanoparticles introduced into lubricants significantly influences pressure distribution, load-carrying capacity, heat generation, and various static and dynamic attributes of hydrodynamic journal bearings. Studies have demonstrated that lubricants contain added nanoparticles.

## 2. Literature Review

Quinci et al. [1] demonstrate that using magnetorheological fluid as a lubricant in a journal-bearing system can result in thicker fluid films at lower speeds and an enhanced pressure distribution. Nonetheless, the increased friction losses observed in the MRF lubricated bearing compared to traditional oil lubrication highlight the complex interplay between various factors in tribological systems. These findings have implications for designing and optimizing bearing systems for specific applications, considering the trade-offs between factors such as viscosity control, pressure distribution, and frictional losses. Gertzos et al. [2] contribute to the understanding of how MR and ER fluids, along with traditional grease, behave in non-Newtonian fluid flow conditions within adaptive journal-bearing systems.

The research highlights the potential for using smart fluids to control bearing behavior dynamically. It provides validation for the accuracy of the 3-D CFD model in predicting fluid behavior in these specialized systems. Satish Sharma et al. [3] examine a specialized journal-bearing design that utilizes micropolar lubricants. By solving a modified Reynolds equation through finite element techniques, the study highlights the benefits of using micropolar lubricants in terms of increased fluid film thickness and decreased friction compared to traditional lubricants. This research contributes to understanding advanced lubrication techniques for improving bearing performance in machinery and mechanical systems. Robert Goraj et al. [4] present an innovative form of bearing that

merges hydrodynamic lubrication and electromagnetic support. By formulating governing equations incorporating gravity, fluid dynamics, and electromagnetic forces, the researchers aim to ascertain the equilibrium positions of the bearing under various loads. Through semi-analytical solutions of the equation system and subsequent validation using the Finite Difference Method, the study offers insights into the performance and stability of this novel bearing design.

This research could have implications for applications where both fluid dynamics and electromagnetic forces play pivotal roles in bearing operation. Bouyer et al. [5] present that integrating real-time monitoring, numerical analysis, and wear forecasting offers a comprehensive approach to managing machine performance and maintenance. This process enables you to anticipate wear-related issues, plan maintenance more effectively, and optimize machine operations for longer lifespans and reduced downtime. Tushar Gundarneeeyya et al. [6] illustrate the favorable effects of incorporating nano lubricants containing Titanium dioxide, copper oxide and aluminum oxide nanoparticles as additives within journal bearings. These nano lubricants' increased viscosity and improved lubrication properties lead to enhanced performance characteristics, including higher maximum pressure and load-carrying capabilities.

This research has practical implications for designing and operating mechanical systems that rely on journal bearings, as nanoparticle additives could contribute to better lubrication, reduced wear, and extended bearing lifespans. Rasep et al. [7] suggest that this research contributes to the understanding of using vegetable oil as an eco-friendly alternative for lubricating journal bearings. By reviewing the efficiency of different oils, considering surface texture modifications, and discussing the broader implications, the study provides insights into this approach's potential benefits and challenges. This research could influence decisions regarding lubricant choices and contribute to more sustainable and efficient machinery operation.

ShashaVali Shaik et al. [8] explore the incorporation of nanoparticles into highly refined mineral-based engine oils to improve their tribological properties. By altering parameters like nanoparticle concentration and applied load and measuring coefficients of wear and friction using a tribometer, the study aims to identify conditions that lead to enhanced lubricant performance. This research can potentially contribute to more efficient and durable machinery operation by reducing friction and wear. Raman Kumar et al. [9] underscore the relevance of using solid lubricants in modern applications that require increased adhesion, low shear strength, and higher compression strength to function optimally in harsh and abrasive conditions. The unique lubricating characteristics of solid lubricants make them a preferred choice in various industries where traditional lubricants might not suffice.

This recognition of solid lubricants' exceptional qualities drives their increased use in emerging technologies and applications. Vineet Sharma et al. [10] highlight how adding graphite particles to lubricating oils can significantly reduce friction coefficients and manage temperature generation during testing. The use of ball milling techniques, blending methods, and tribometer testing contributes to understanding how graphite additives enhance lubrication properties. This research has implications for optimizing lubricant formulations to improve mechanical systems' friction-reduction performance. Qin Dong et al. [11] focus on assessing the fatigue strength of journal-bearing examples using tin-based Babbitt bushes. The author employs a fluid-structure interaction approach, simulating oil film pressure and considering cavitation effects. The simulation results are validated through experiments conducted on hydraulic servo dynamic fatigue testing equipment.

The significant consistency between the simulation and experimental results affirms the accuracy of the fatigue strength evaluation approach. Wenjie Zhou et al. [12] introduce a novel numerical approach for studying the lubricated characteristics of journal bearings. This approach combines the finite element method for solving the static Reynolds equation and the mixed method for finding the equilibrium position of the bearings. The study validates the new model by comparing its results to those of a previous model that used the finite difference technique. The accuracy and reliability of the new numerical method are assessed through the analysis of relative error margins compared with the prior model. Lubos Smolik et al. [13], explores the effects of mechanically indented textures on the stability of lightly loaded journal bearings, specifically in applications like vertical rotors and microturbines. The study emphasizes the sensitivity of numerical solutions to computational mesh density and proposes the use of a reduced cavitation approach to address this issue. This approach is particularly useful for scenarios where CPU time is limited, enabling efficient optimization, iterative methods, and solving equations of motion. The research findings provide valuable insights into optimizing the analysis of textured journal bearings in practical applications.

Alexey Kornaev et al. [14] examine the viscosity wedge effect and its influence on hydrodynamic lubrication in lightly loaded fluid-film bearings. The study combines theoretical analysis and experimental validation to explore the optimization of viscosity distribution and its impact on shaft vibrations and friction coefficients. The findings suggest that the viscosity wedge effect can positively influence lubrication performance, as supported by theoretical and practical results. This research contributes to understanding lubrication mechanisms and optimization techniques for fluid-film bearings. Jongin Yang et al. [15], presents an advanced approach to studying granular lubrication performance using Computational Fluid

dynamics. By utilizing an enhanced theoretical modeling approach rooted in the Euler-Eulerian multiphase flow model and the solid kinetic theory, the study enhances our understanding of granular lubrication systems. Including a parametric analysis and validation against experimental data further strengthens the model's credibility. The insights gained from the analysis have practical implications for designing effective and efficient granular lubrication systems in various applications. Bassam Alshaer et al [16], delves into the mixed lubrication performances and critical characteristics of water-lubricated bearings under extreme conditions. The study introduces a novel multi-field coupling lubrication model and establishes functional mapping linkages between lubrication performance and influencing parameters. Rotor dynamic models with surface microtopography are used to explain dynamic behavior variations. The theoretical analysis is validated through experiments, showcasing the model's and algorithms' reliability.

The research contributes to a comprehensive understanding of water-lubricated bearing behavior and provides insights into optimizing their performance in challenging conditions. Zhongliang Xie et al. [17], focuses on the tribological behavior and dynamic characteristics of a textured journal-thrust coupled bearing. The author develops a TEHD lubrication analysis model that considers both thermal and pressure-coupled effects. This model incorporates flow, pressure, and thermal continuity conditions between different bearing parts. The experimental validation, carried out using specialized testing equipment, supports the model's validity and accuracy. Overall, the research contributes to a deeper understanding of the behavior of textured journal-thrust coupled bearings under the influence of thermal and pressure effects. Shaoyu Zhu et al [18], presents a new concept for a flexible Temperature-Control Curtain (TCC) and investigates its potential engineering applications. The paper focuses on the thermal structure and hydrodynamic characteristics of the proposed TCC scheme. Through a combination of structural nonlinear analysis and the VFIFE method, a three-dimensional form of the TCC is obtained. The theoretical modeling and analysis work provides essential references for future engineering operations. Overall, the research contributes to the understanding and potential utilization of the new flexible TCC scheme in engineering contexts.

Chellapandi et al [19], investigates the wear parameters of journal sliding bearings when operated under contaminated water lubrication conditions. Through experimental examinations, the author analyzes the effects of various factors, including bearing materials and lubricating groove layouts. The results of the studies highlight the notable influence of water pollution on the wear characteristics of the bearing system parts. This research contributes to a better understanding of the impact of contaminated water on bearing wear and emphasizes the

importance of proper lubrication practices in such a scenario. Bouyer et al [20]. This approach considers the combined influences of a double-layer porous structure and the behavior of a non-Newtonian lubricant (described by the cubic law model). The study examines how the interplay between factors such as the non-linear lubricant properties, permeability parameter, and semi-cone angle affects the bearing's performance. In the case of the hybrid DCPB, the researcher employed a finite element approach to solve the modified Reynolds equation. The findings indicate that DCPB outperforms the hybrid Single layer Conical Porous Bearing (SCPB) regarding performance metrics. Nino Dakov [21]. The research paper titled "A study of double layer conical porous hybrid journal bearing operated with non-Newtonian lubricant" explores the performance of a hybrid Double layer Conical Porous Bearing (DCPB) utilizing a non-Newtonian lubricant. The author proposes a numerical simulation approach to study this system, considering the combined effects of a double-layer porous matrix and non-Newtonian lubricant behavior.

Anil Singh et al. [22]. discusses the importance of hydrodynamic lubrication and specifically addresses the analysis of non-Newtonian fluids in this context. The author introduces calculation methods for deriving equations related to non-Newtonian hydrodynamic lubrication, focusing on the separated flow velocity method. The paper provides readers with basic equations, numerical calculation methodologies, and practical programs that can be utilized for analyzing both one-dimensional and two-dimensional hydrodynamic lubrication involving non-Newtonian fluids. This research contributes to the understanding and application of lubrication principles in scenarios where non-Newtonian fluid behavior is a significant factor. Hussein Sayed et al [23]. delves into the hydrodynamic lubrication performance of bionic multi-scale composite surface textures inspired by natural patterns. The author designs six such textures and employs numerical simulation to analyze how geometric parameters and service conditions influence lubrication characteristics. The results likely indicate that the bionic textures enhance load-carrying capacity and reduce friction coefficient, with groove combinations offering better lubrication performance compared to wavy combinations. This research contributes to understanding bio-inspired texture design for improved lubrication characteristics.

Long Zheng et al. [24]. explores the failure analysis of the auxiliary support bearing and shaft tribopair in a seawater hydraulic axial piston pump. The auxiliary support structure's role in preventing cylinder block tilting is explained. The paper compares failure modes under different material combinations and highlights the impact of radius fitting clearance design. The running-in experiment conducted under optimized conditions demonstrates improved pump performance and reduced wear on friction pair surfaces. Ultimately, the research offers guidance for

designing auxiliary support bearings in SHAPP, enhancing its operational reliability and performance. Shengbo Li et al. [25]. introduces an innovative analytical solution for determining the dynamic characteristics of lubricated long journal bearings under dynamic loading conditions. This solution is developed by integrating Reynold's equation, including equations for evaluating lubricant dynamic forces and zero pressure angles. The new solution is applied to practical examples, and the results are compared with those obtained using Gumbel's solution. Ultimately, the research paper contributes to the field of lubrication dynamics by offering an exact analytical method for analyzing the behavior of lubricated long journal bearings under dynamic loads.

Hussein Sayed et al [26]. addresses the importance of hydrodynamic lubrication and its application to non-Newtonian fluids scenarios. The author introduces calculation methods based on the hydrodynamic lubrication equation derived using the separated flow velocity method. The paper provides essential equations, numerical calculation methodologies, and practical programs for both one-dimensional and two-dimensional hydrodynamic lubrication cases. This research contributes to a deeper understanding of lubrication dynamics in situations where non-Newtonian fluid behavior is a key factor and provides practical tools for engineers to analyze and optimize lubrication performance in various applications. Muhammad Imran Sadiq et al. [28] contribute to understanding how misaligned journal bearings behave under heavy loads while lubricating with non-Newtonian fluids. Using a pseudoplastic lubricant and considering surface roughness adds complexity to the lubrication scenario. By deriving a generalized average Reynolds equation and employing numerical methods, the paper offers insights into the performance of these bearings. Furthermore, the paper emphasizes how surface roughness can mitigate certain negative effects, contributing to the overall understanding of bearing behavior in challenging conditions.

Shaswat Saincher et al. [29] enhance the comprehension of the dynamic traits of rotor systems equipped with pocket bearings. commonly found in sodium-cooled fast reactor coolant pumps. By combining hydrostatic and hydrodynamic effects, these bearings exhibit hybrid characteristics. The paper introduces a numerical analysis approach and a stability chart for rotor dynamics, which holds relevance for real-world applications. The research underscores the benefits of pocket-type bearings in terms of stability control and lower added fluid mass. Finally, the numerical tool's accuracy is validated through experimental measurements, providing confidence in its application to real-world scenarios. Songlin Nie et al. [31]. Explores the assessment of the performance of a thrust bearing featuring hydrostatic lift pockets. Through experiments conducted under various lubrication modes (hydrostatic, hybrid, and hydrodynamic),

the study demonstrates the positive impact of hydrostatic lubrication on the bearing’s load-carrying capacity and overall performance. The research highlights the significance of different lubrication modes in enhancing the behavior of thrust bearings and contributes to understanding bearing dynamics and lubrication strategies.

Huanhuan Wang et al. [32] focuses on the soft elastohydrodynamic analysis of radial oil seals with hydrodynamic pumping structures. Through the introduction of advanced sub-models, the paper accounts for key factors such as elastic deformation and pressure buildup. By analyzing back-pumping flow and surface deformation, the research contributes to understanding how these elements impact the behavior of the oil seal. Calculating pumping rate and friction torque further provides valuable insights into the overall performance of the radial oil seal with hydrodynamic features.

### 3. Materials and Methods

The experimentation described involves testing on a journal-bearing test rig in four distinct stages. The experiments are conducted using SAE30 oil and nano ferro fluids with varying concentrations (15%, 20%, and 25%) under different loads and rotational speeds. The objective is to gather data and obtain design parameters for different oils using mathematical form. The main goal of this experiment is to evaluate how journal bearings perform when subjected to various operating conditions and different types of fluids.

By gathering data, calculating relevant parameters, and comparing outcomes to determine how various factors influence the behavior of the bearing system. The inclusion of pressure distribution curves provides a visual representation of how pressure is distributed across the bearing surfaces. The results and findings from this experimentation contribute to understanding the impact of fluid type, concentration, load, and rotational speed on the performance of the journal-bearing system.

Test Rig and its Specifications are mentioned below,

Journal Diameter (A) 2R	=	55mm
Bearing Diameter (E) 2r	=	70mm
Width (L)	=	15mm
Bearing weight when attached	=	1.7kg
DC Motor	=	0.5HP
DC Motor	=	1500rpm

Speed fluctuation is accommodated via a dimmer stater to run journal at required speeds and adjust the fluid levels in the manometer tubes. A 16-tube manometer board with sufficient height, appropriate scales, and an adjustable oil tank are attached with a hydrodynamic journal-bearing test rig upon which the experiment will be performed.



Fig. 1 Hydrodynamic journal bearing test rig

Table 1. Parameters and levels

Parameters/ Levels	Level 1	Level 2	Level 3
Load (W)	100	150	200
Speed (N)	500	600	700

Table 1 outlines the parameters and levels considered using the Taguchi method. The study focuses on two parameters, each with three levels. This approach helps systematically analyze and optimize the experimental setup for efficient data collection and analysis.

By utilizing the Taguchi method and designing the experiments with a systematic approach to parameter variation can efficiently Examine the impacts of varying load and speed conditions on the observed outcomes of interest. This structured experimentation helps in understanding the behavior and performance of the system under various operational scenarios.

Table 2. Lubricants considered: SAE 30 oil, Nano Ferro Fluids (NFF) of 15%, 20 % and 25 % concentration

S. No	Oil type	Properties	Values
1	SAE 30 oil	Density (g/m <sup>3</sup> )	0.86
		Dynamic Viscosity(cp)	7.4
2	NFF 15%	Density(g/m <sup>3</sup> )	0.85
		Dynamic Viscosity(cp)	16
3	NFF 20%	Density(g/m <sup>3</sup> )	0.85
		Dynamic Viscosity(cp)	17
4	NFF 25%	Density(g/m <sup>3</sup> )	0.85
		Dynamic Viscosity(cp)	18

Table 2 offers a comprehensive overview of the characteristics of each employed lubricant in the study. These properties are pivotal in influencing the behavior and efficacy of the lubricants within the experimental framework. This information is useful for analyzing how variations in lubricant properties impact the study’s outcomes, particularly to load, speed, and other parameters being investigated.



Fig. 2 Nano ferro fluids used

### 3.1. Calculations

#### 3.1.1. Length of the Bearing

Diameter of the journal (d) is 55mm. We know from the design values of journal bearing that the ratio of l/d for journal varies from 1 to 2.

Let us take l/d=1.6,

$$l = 1.6 d = 1.6 \times 55 = 88 \text{ mm.}$$

#### 3.1.2. Bearing Pressure

$$P = w(l \times d) = 20.59 / (88 \times 55) = 0.004254132 \text{ N/mm}^2$$

$$\begin{aligned} \text{Bearing load at N rpm} &= \text{Bearing wt. in dry condition} + \\ &\quad \text{Balancing load Wt.} + \text{Added Wt.} \\ &= 1.7 + 2 \times 0.150 + 0.10 = 2.1 \text{ kg} = 20.59 \text{ N.} \end{aligned}$$

#### 3.1.3. Bearing Modulus

Absolute viscosity of SAE 30 oil at a temperature of 38°C is taken from the standard machine design data book. Absolute viscosity (Z)=0.078 and N=500 rpm P=0.004254132 Nmm<sup>2</sup>, Therefore

$$ZNP/p = ((0.078 \times 500)) / 0.004254132 = 9167.5$$

$$ZN/p = 9.16 \times 10^3$$

We consider the operating value from the standard machine design data book, ZN/P=28. The minimum value of the bearing modulus at which the oil film will break is obtained by 3k=ZN/P; therefore, the Bearing Modulus at the minimum point of friction,  $k = 1/3(ZN/p) = 1/3 \times 28 = 9.33$

The bearing will operate under hydrodynamic conditions when the calculated value of the journal bearing characteristic number is above 9.

#### 3.1.4. Coefficient of Friction

$$\mu = 33/10^8 [zN/P][d/c] + k \quad (1)$$

Where, bearing characteristic number (Z) is in kg/m-s, bearing pressure (P) is in N/mm<sup>2</sup>, k = factor to correct for end leakage. The factor to correct the end leakage (k) depends upon the ratio of length to the diameter of the

bearing (i.e., l/d). k = 0.002 for l/d ratios of 0.75 to 2.8,

$$\begin{aligned} \mu &= 33 / (10^8 [(9.16 \times 10^3)] [1 / 0.00545]) + 0.002 \\ \mu &= 0.0564 \end{aligned}$$

#### 3.1.5. Sommerfeld Number

$$\text{Sommerfeld number} = zN / (P(d/c)^2) \quad (2)$$

For design purposes, its value is taken,

$$zN/P (d/c)^2 = 14.3 \times 10^6$$

But for  $zN/P = 9.16 \times 10^3$  and  $(d/c) = 1/0.0545$

We get, Sommerfeld number =  $2.9 \times 10^6$

#### 3.1.6. The Heat Generated within the Bearing

$$Qg = \mu wv \text{ watts} \quad (3)$$

Where,  $\mu = 0.0564$ , and W = load on, the bearing in N = bearing pressure in N/mm<sup>2</sup> x area of the bearing in mm<sup>2</sup>

Therefore

$$w = P(l \times d) = 0.004254132(88 \times 55) \times 9.81$$

$$W = 20.5899 \text{ N}$$

v = rubbing velocity in m/s =  $\pi dN/60$ ,

$$v = \pi \times 0.05 \times 500 / 60 = 1.430 \text{ m/s}$$

Therefore,  $Qg = 0.0564 \times 20.5899 \times 1.430 =$

$$1.662 \text{ watts or N - m/s}$$

#### 3.1.7. Heat Dissipated by the Bearing

$$Qd = C.A(t_b - t_a) / s \text{ or } W \quad (4)$$

Where, C = coefficient for heat dissipation in W/m<sup>2</sup>/°C,

A = Bearing area in m<sup>2</sup> = l x d,

t<sub>b</sub> = bearing surface temperature in °C, and

t<sub>a</sub> = Temperature of the surrounding air at °C,

Average value of C is considered as:

Un = ventilated bearings = 140 to 420 W/m<sup>2</sup>/°C,

Well = ventilated bearings = 490 to 1400 W/m<sup>2</sup>/°C,

Since our bearing is well-ventilated bearing, we take the value as 1232,

$$Q_d = c.l.d(t_b - t_a) = 140 \times 0.008 \times 0.005(39 - 29)$$

$$Q_d = 4.06 \text{ watts}$$

#### 3.1.8. Critical Pressure of the Bearing

Critical pressure or minimum operating pressure is

$$p = zN / 4.75 \times 10^6 (d/c)^2 (l/d + 1)$$

$$p = 0.078 \times 500 / 4.75 \times 10^6 (1/0.00540)^2 (88/55 + 88) \text{ N/mm}^2,$$

Therefore, p=0.001637 N/mm<sup>2</sup>.

Similarly, the experiment is repeated for 600 and 700 rpms for loads 100gm, 150gm, and 200gm for different fluids and respective design parameters are calculated. In order to make a calculation faster, a C Program is written to do the calculations.

**Table 3. Design parameters values for different loads and speeds for SAE30 oil**

(W, N)	L	P	C=ZN/P	$\mu$	S	$Q_g$	$Q_d$	p
(100,500)	88	0.00425	9167	0.0564	$2.9 \times 10^6$	1.662	4.06	0.00163
(150,500)	88	0.00439	8988	0.0553	$2.9 \times 10^6$	1.663	4.74	0.00163
(200,500)	88	0.00454	8580	0.0529	$2.7 \times 10^6$	1.666	5.42	0.00163
(100,600)	88	0.00425	11001	0.0673	$3.5 \times 10^6$	2.385	4.73	0.00796
(150,600)	88	0.00433	10786	0.0660	$3.4 \times 10^6$	2.386	4.06	0.00796
(200,600)	88	0.00454	10296	0.0631	$3.3 \times 10^6$	2.389	4.74	0.00796
(100,700)	88	0.00425	12834	0.0782	$4.15 \times 10^6$	3.221	6.77	0.00229
(150,700)	88	0.00433	12584	0.0767	$4 \times 10^6$	3.223	8.13	0.00229
(200,700)	88	0.00454	12012	0.0733	$3.8 \times 10^6$	3.227	8.15	0.00229

**Table 4. Design parameters values for different loads and speeds for nano ferrofluid with 15% concentration oil**

(W, N)	L	P	C=ZN/P	$\mu$	S	$Q_g$	$Q_d$	p
(100,500)	88	0.00425	1880	0.0131	$0.6 \times 10^6$	0.382	2.71	0.00033
(150,500)	88	0.00433	1843	0.0129	$0.59 \times 10^6$	0.388	2.83	0.00033
(200,500)	88	0.00454	1760	0.0124	$0.57 \times 10^6$	0.391	4.06	0.00033
(100,600)	88	0.00425	2256	0.0154	$0.73 \times 10^6$	0.545	2.71	0.00040
(150,600)	88	0.00433	2212	0.0151	$0.71 \times 10^6$	0.546	2.94	0.00040
(200,600)	88	0.00454	2212	0.0145	$0.68 \times 10^6$	0.550	3.38	0.00040
(100,700)	88	0.00425	2632	0.0176	$0.85 \times 10^6$	0.726	4.74	0.00047
(150,700)	88	0.00433	2581	0.0173	$0.83 \times 10^6$	0.729	4.74	0.00047
(200,700)	88	0.00454	2464	0.0166	$0.79 \times 10^6$	0.731	4.74	0.00047

**Table 5. Design parameters values for different loads and speeds for nano ferro fluid with 20% concentration oil**

(W, N)	L	P	C=ZN/P	$\mu$	S	$Q_g$	$Q_d$	p
(100,500)	88	0.00425	1998	0.0138	$0.64 \times 10^6$	0.408	4.74	0.00035
(150,500)	88	0.00433	1959	0.0136	$0.63 \times 10^6$	0.409	4.86	0.00035
(200,500)	88	0.00454	1760	0.0124	$0.57 \times 10^6$	0.391	4.94	0.00035
(100,600)	88	0.00425	2397	0.0162	$0.77 \times 10^6$	0.575	5.42	0.00042
(150,600)	88	0.00433	2350	0.0159	$0.76 \times 10^6$	0.576	4.06	0.00048
(200,600)	88	0.00454	2244	0.0153	$0.72 \times 10^6$	0.580	3.38	0.00042
(100,700)	88	0.00425	2797	0.0186	$0.90 \times 10^6$	0.766	4.73	0.00050
(150,700)	88	0.00433	2740	0.186	$0.88 \times 10^6$	0.768	4.06	0.00050
(200,700)	88	0.00454	2618	0.0175	$0.84 \times 10^6$	0.772	3.33	0.00050

Table 3 provides experimental data and calculated values of SAE 30oil for various parameters related to bearing performance. Each row represents a specific combination of Load (W) and Speed (N), and the corresponding values for parameters such as Bearing Pressure (P), Bearing Characteristic Number (C), Coefficient of Friction ( $\mu$ ), Sommerfeld Number (S), Heat Generated ( $Q_g$ ), Heat Dissipated ( $Q_d$ ), and Critical Pressure (p). Each row corresponds to a specific load and speed value set, and the corresponding calculated parameters are provided in the respective columns. This data provides valuable insights into how the bearing performs under different load and speed conditions and the resulting effects on the various calculated parameters.

Table 4 provides experimental data and calculated values of nano ferro fluids 15 % Concentration for various parameters related to bearing performance. Each row represents a specific combination of Load (W) and Speed (N), and the corresponding values for parameters such as Bearing Pressure (P), Bearing Characteristic Number (C), Coefficient of Friction ( $\mu$ ), Sommerfeld Number (S), Heat Generated ( $Q_g$ ), Heat Dissipated ( $Q_d$ ), and Critical Pressure (p). Each row corresponds to a specific load and speed value set, and the corresponding calculated parameters are provided in the respective columns. This data provides valuable insights into how the bearing performs under different load and speed conditions and the resulting effects on the various calculated parameters.

**Table 6. Design parameters values for different loads and speeds for nano ferro fluid with 25 % concentration oil**

(W, N)	L	P	C=ZN/P	$\mu$	S	$Q_g$	$Q_d$	p
(100,500)	88	0.00425	2115	0.0145	$0.68 \times 10^6$	0.428	3.38	0.000378
(150,500)	88	0.00433	2074	0.0143	$0.63 \times 10^6$	0.430	3.42	0.000378
(200,500)	88	0.00454	1980	0.0137	$0.64 \times 10^6$	0.432	4.06	0.000378
(100,600)	88	0.00425	2538	0.0170	$0.82 \times 10^6$	0.604	4.73	0.000453
(150,600)	88	0.00433	2489	0.167	$0.80 \times 10^6$	0.606	4.74	0.000453
(200,600)	88	0.00454	2376	0.161	$0.76 \times 10^6$	0.609	4.78	0.000453
(100,700)	88	0.00425	2961	0.0195	$0.95 \times 10^6$	0.806	4.74	0.00052
(150,700)	88	0.00433	2904	0.192	$0.94 \times 10^6$	0.808	4.42	0.00052
(200,700)	88	0.00454	2772	0.0184	$0.89 \times 10^6$	0.812	4.06	0.00052

Table 5 provides experimental data and calculated values of nano ferro fluids 20 % Concentration for various parameters related to bearing performance. Each row represents a specific combination of Load (W) and Speed (N), and the corresponding values for parameters such as Bearing Pressure (P), Bearing Characteristic Number (C), Coefficient of Friction ( $\mu$ ), Sommerfeld Number (S), Heat Generated ( $Q_g$ ), Heat Dissipated ( $Q_d$ ), and Critical Pressure (p). Each row corresponds to a specific load and speed value set, and the corresponding calculated parameters are provided in the respective columns. This data provides valuable insights into how the bearing performs under different load and speed conditions and the resulting effects on the various calculated parameters.

Table 6 provides experimental data and calculated values of nano ferro fluids 25 % Concentration for various parameters related to bearing performance. Each row represents a specific combination of Load (W) and Speed (N), and the corresponding values for parameters such as Bearing Pressure (P), Bearing Characteristic Number (C), Coefficient of Friction ( $\mu$ ), Sommerfeld Number (S), Heat Generated ( $Q_g$ ), Heat Dissipated ( $Q_d$ ), and Critical Pressure (p). Each row corresponds to a specific load and speed value set, and the corresponding calculated parameters are provided in the respective columns. This data provides valuable insights into how the bearing performs under different load and speed conditions and the resulting effects on the various calculated parameters.

#### 4. Results and Discussion

The hydrodynamic journal bearing test rig is first filled with Castrol SAE 30 oil, and the journal bearing is operated at 500 rpm with a suspended load of 100 N. Manometer tubes have pressure levels ranging from 6.5cm to 123.1cm (Figure 3). When nano ferro fluids with 15%, 20%, and 25% concentrated lubricants are employed, pressure levels in manometer tubes vary from 35cm to 65.5cm, 35.25cm to 63.75cm, and 35.5cm to 68cm (Figure 4, 5, and 6). When pressure levels in manometer tubes are compared to SAE 30

oil, it is obvious that nano ferro fluids with 15%, 20%, and 25% concentrations have reduced pressure variation levels. When the hydrodynamic journal bearing test rig is initially filled with Castrol SAE 30 oil and the journal bearing, the system operates at a maximum speed of 700 rotations per minute (rpm) while supporting a hanging load of 200 N (Newtons). The values of journal-bearing design parameters such as bearing characteristic number, coefficient of friction, Somerfield number, and heat generation are 12012, 0.0733,  $3.8 \times 10^6$ , and 3.227, respectively.

When nano ferro fluids with 15%, 20%, and 25% concentrated lubricants are used then bearing character numbers of 2464, 2618, and 2772 and coefficient of friction values of 0.0166, 0.0175, 0.0184, and heat generation values of 0.731, 0.772, 0.812 are obtained. The provided information outlines the changes in pressure variation levels when using different lubricants and concentrations. It also highlights the impact of lubricants on bearing design parameters under varying conditions. The description effectively demonstrates the experimental setup and the resulting effects on bearing performance.

The below graph depicts the pressure fluctuation at different manometer tube inlets, with the least pressure occurring at the 9th tube inlet and the greatest pressure occurring at the D tube intake, with pressure values ranging from 6.5 cm to 123.1 cm for SAE-30 oil. When the journal bearing works at 500 rpm, and a load of 100 N, graphs are shown between the pressure distribution on the Y-axis and the circumferential tube inlet angles on the X-axis. The graph depicts pressure fluctuations at different manometer tube inlets and visually represents how pressure varies across different manometer tube inlets, indicating both the highest and lowest pressure points. The pressure values are provided for each point, and the X-axis showcases the corresponding circumferential tube inlet angles. This graph provides valuable insights into pressure distribution under specific operating conditions, offering a clear visualization of the pressure variations across the bearing system.

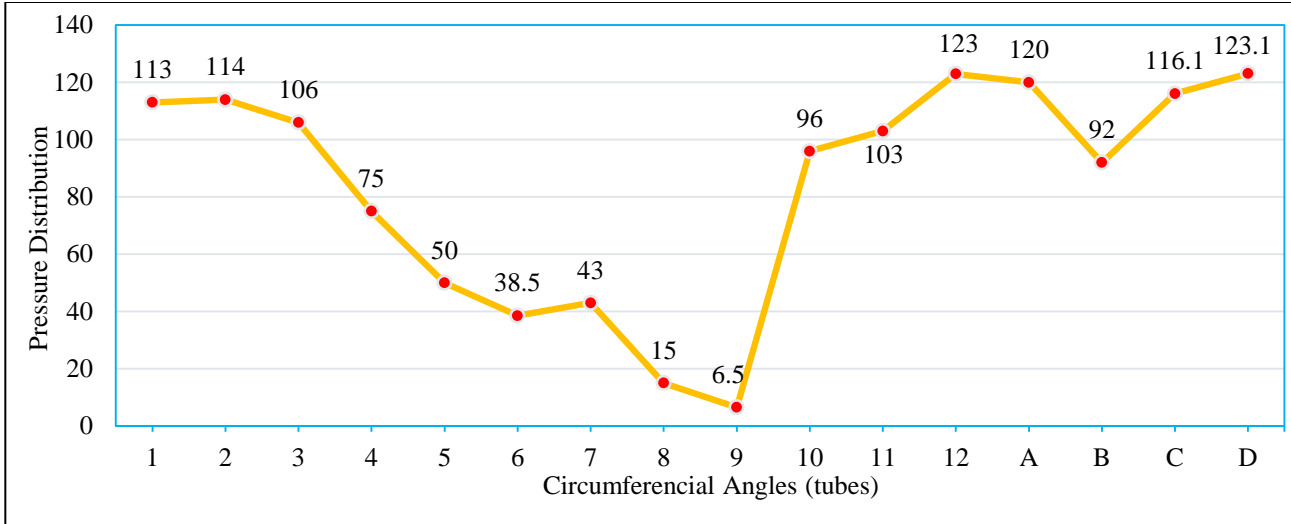


Fig. 3 Pressure distribution at various inlet points for SAE 30 oil

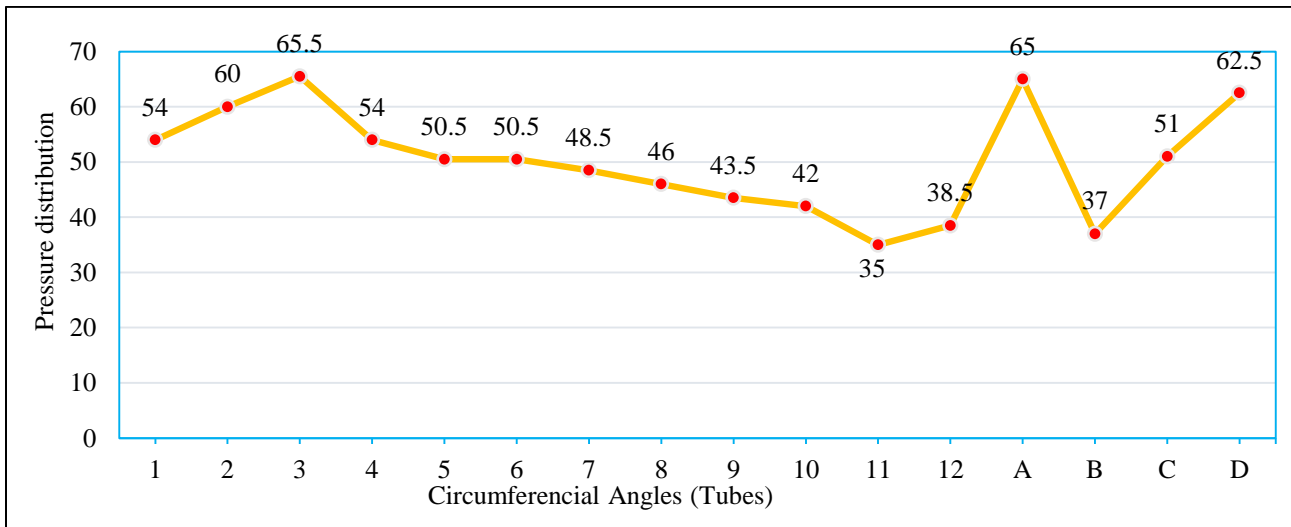


Fig. 4 Pressure distribution at various inlet points for nano ferro fluid 15% concentration oil

The above graph depicts the pressure fluctuation at different manometer tube inlets, with the least pressure occurring at the 11<sup>th</sup> tube inlet and the greatest pressure occurring at the 3<sup>rd</sup> tube intake, with pressure values ranging from 35 cm to 65.5 cm for Nano ferro fluid with 15 % concentration. When the journal bearing works at 500 rpm, and a load of 100 N, graphs are shown between the pressure distribution on the Y-axis and the circumferential tube inlet angles on the X-axis. The graph depicts pressure fluctuations at different manometer tube inlets and visually represents how pressure varies across different manometer tube inlets, indicating both the highest and lowest pressure points. The pressure values are provided for each point, and the X-axis showcases the corresponding circumferential tube inlet angles. This graph provides valuable insights into pressure distribution under specific operating conditions, offering a clear visualization of the pressure variations across the bearing system.

The below graph depicts the pressure fluctuation at different manometer tube inlets, with the least pressure occurring at the 11<sup>th</sup> tube inlet and the greatest pressure occurring at the 3<sup>rd</sup> tube intake, with pressure values ranging from 35.25 cm to 63.75 cm for Nano ferro fluid with 20 % concentration. When the journal bearing works at 500 rpm, and a load of 100 N, graphs are shown between the pressure distribution on the Y-axis and the circumferential tube inlet angles on the X-axis. The graph depicts pressure fluctuations at different manometer tube inlets and visually represents how pressure varies across different manometer tube inlets, indicating both the highest and lowest pressure points. The pressure values are provided for each point, and the X-axis showcases the corresponding circumferential tube inlet angles. This graph provides valuable insights into pressure distribution under specific operating conditions, offering a clear visualization of the pressure variations across the bearing system.

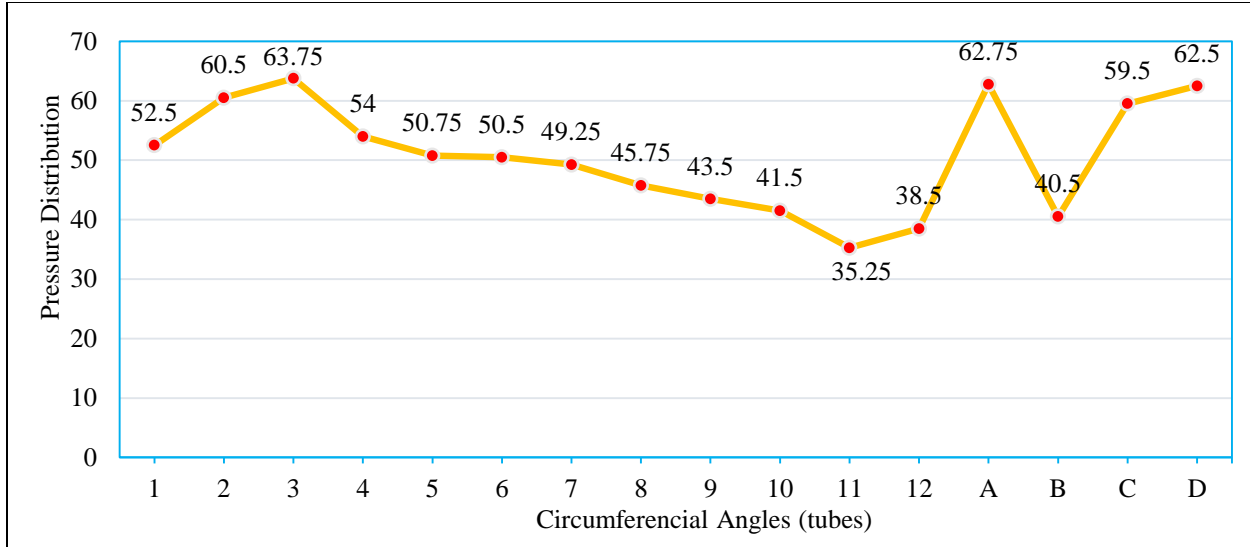


Fig. 5 Pressure distribution at various inlet points for nano ferro fluid 20 % concentration oil

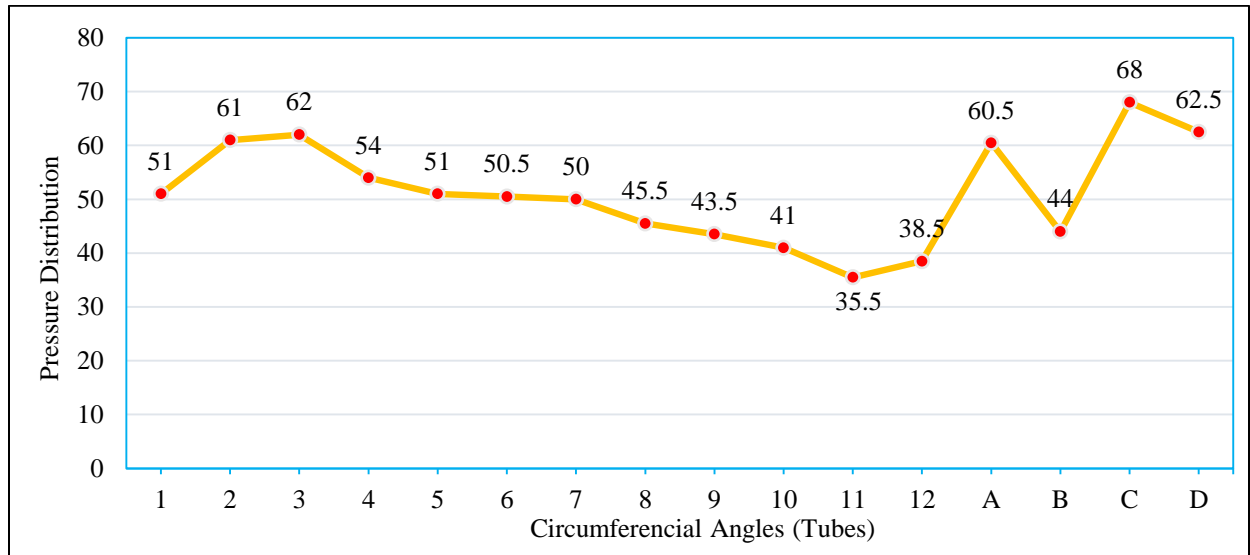


Fig. 6 Pressure distribution at various inlet points for nano ferro fluid 25% concentration oil

The above graph depicts the pressure fluctuation at different manometer tube inlets, with the least pressure occurring at the 11<sup>th</sup> tube inlet and the greatest pressure occurring at the 3<sup>rd</sup> tube intake, with pressure values ranging from 35.5 cm to 68 cm for Nano ferro fluid with 25 % concentration. When the journal bearing works at 500 rpm, and a load of 100 N, graphs are shown between the pressure distribution on the Y-axis and the circumferential tube inlet angles on the X-axis. The graph depicts pressure fluctuations at different manometer tube inlets and visually represents how pressure varies across different manometer tube inlets, indicating both the highest and lowest pressure points. The pressure values are provided for each point, and the X-axis

showcases the corresponding circumferential tube inlet angles. This graph provides valuable insights into pressure distribution under specific operating conditions, offering a clear visualization of the pressure variations across the bearing system.

The combined graph of pressure distribution curves (Figure 7) shows that, as compared to the SAE oil curve, nano ferro fluid curves have less pressure on bearing. Among the nano ferro fluids, 15% concentration fluid has lower pressure than 20% and 25% concentration fluids. Finally, it is clear that adding 15% nano ferro particles to basic lubricating oil improves bearing pressure levels.

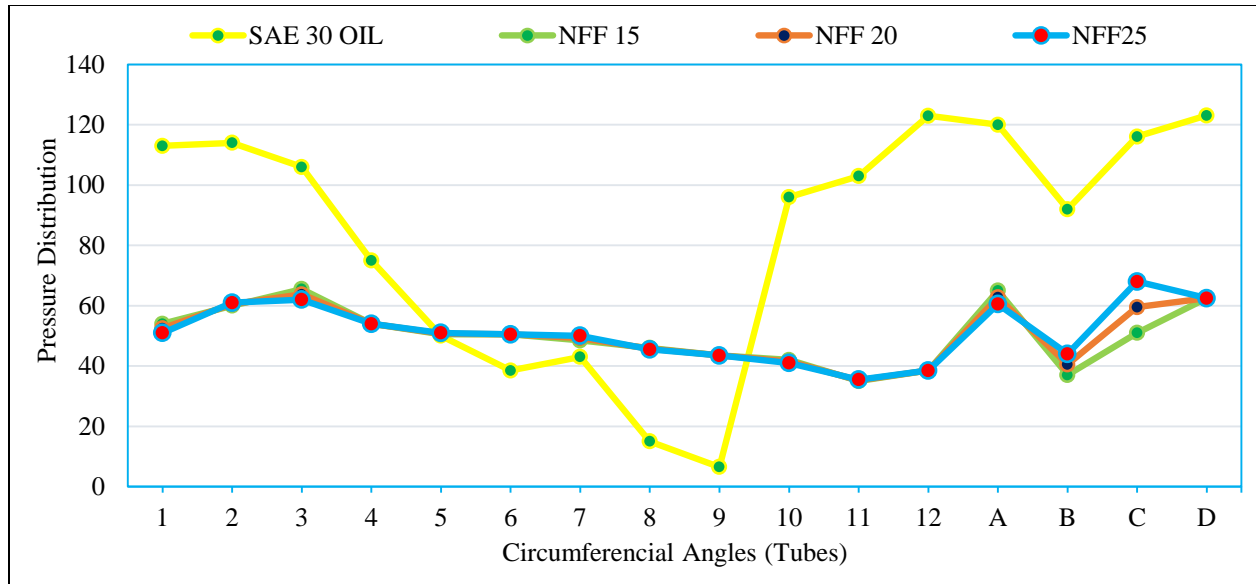


Fig. 7 Combined pressure distribution curves for SAE 30 oil, nano ferro fluids 15 %, 20% and 25 % concentration oil

Table 7. Comparison of bearing characteristic number at maximum loads and speeds for SAE 30 oil and nano ferro fluid with different concentration's

Type of Fluids	Bearing Characteristic Number (C = ZN/P)
SAE 30 Oil	12012
Nano Ferro Fluid with 15% Concentration	2464
Nano Ferro Fluid with 20% Concentration	2618
Nano Ferro Fluid with 25% Concentration	2772

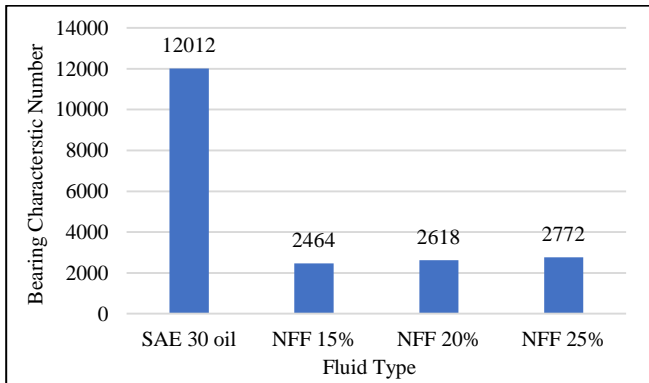


Fig. 8 Graphical representation of bearing characteristics number for SAE 30 oil, nano ferro fluids 15 %, 20% and 25 % concentration oil

Table 7 illustrates the Bearing Characteristic Number (C = ZN/P) for different types of fluids. The bearing characteristic number for SAE 30 oil is 12012, which is lowered to 2464 with the addition of 15% nanoparticles, and 2618 and 2772 with the addition of 20% and 25% concentrations, respectively. As using nano ferro fluids, the characteristic

number is reduced as compared to SAE 30 oil the bearing characteristic number is a crucial parameter that reflects the performance of a bearing system under specific operating conditions and lubricants. The provided data shows how fluid type and concentration can significantly affect this parameter, potentially influencing the bearing's behavior and performance. The graph describes the bearing characteristic number for SAE 30 oil as 12012; with the addition of nanoparticles of 15 % concentration, it is reduced to 2464; similarly, with the addition of 20% and 25% concentrations, it is reduced to 2618 and 2772, respectively.

Table 8. Comparison of coefficient of friction at maximum loads and speeds for SAE 30 oil and nano ferro fluid with different concentration's

Type of Fluids	Coefficient of Friction ( $\mu$ )
SAE 30 Oil	0.0733
Nano Ferro Fluid with 15% Concentration	0.0166
Nano Ferro Fluid with 20% Concentration	0.0175
Nano Ferro Fluid with 25% Concentration	0.0184

Table 8 offers a comparison of the coefficient of friction ( $\mu$ ) at maximum loads and speeds for different types of fluids, SAE 30 oil and Nano Ferro Fluid with various concentrations. Moreover, the coefficient of friction for SAE 30 oil is 0.0733, which is lowered to 0.0166 with the addition of 15% nanoparticles and 0.0175 and 0.184 with the addition of 20% and 25% concentrations, respectively, using nano ferro fluids, the characteristic number is reduced as compared to SAE 30 oil. The coefficient of friction is a significant parameter that indicates the level of friction between two surfaces.

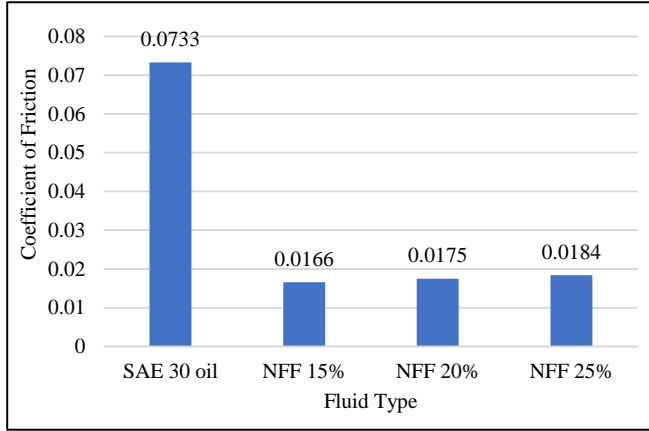


Fig. 9 Graphical representation of coefficient of friction for SAE 30 oil, nano ferro fluids 15 %, 20% and 25 % concentration oil

The provided data demonstrates how different types of fluids and their concentrations can have varying effects on the coefficient of friction, affecting the bearing system’s performance and efficiency. The lower friction coefficients for nano ferro fluids with different concentrations suggest improved lubricating properties compared to SAE 30 oil.

The graph describes the coefficient of friction for SAE 30 oil as 0.0733 with the addition of nanoparticles of 15% concentration; it is reduced to 0.0166; similarly, with the addition of 20% and 25% concentrations, it is reduced to 0.0175 and 0.0184 respectively.

Table 9. Comparison of somerfield number at maximum loads and speeds for SAE 30 oil and nano ferrofluid with different concertations

Type of Fluids	Somerfield Number (S)
SAE 30 Oil	$3.8 \times [10]^6$
Nano Ferro Fluid with 15% Concertation	$0.79 \times [10]^6$
Nano Ferro Fluid with 20% Concertation	$0.84 \times [10]^6$
Nano Ferro Fluid with 25% Concertation	$0.89 \times [10]^6$

Table 9 shows the comparison of the Sommerfeld Number (S) at maximum loads and speeds for different types of fluids: SAE 30 oil and Nano Ferro Fluid with various concentrations; the Somerfield number for SAE 30 oil is  $3.8 \times 10^6$ , which is lowered to  $0.79 \times 10^6$  with the addition of 15% nanoparticles, and  $0.84 \times 10^6$  and  $0.84 \times 10^6$  with the addition of 20% and 25% concentrations, respectively as using nano ferro fluids, the Somerfield number is reduced as compared to SAE 30 oil.

The Sommerfeld Number is a fundamental parameter utilized to evaluate the stability of a journal bearing and anticipate its operational performance. The provided data illustrates how different types of fluids and their concentrations

can lead to significant variations in the Sommerfeld Number, which reflects the lubricating ability and effectiveness of the fluids in maintaining a stable bearing operation. The lower Sommerfeld Numbers for nano ferro fluids with different concentrations suggest that these fluids contribute to improved stability compared to SAE 30 oil.

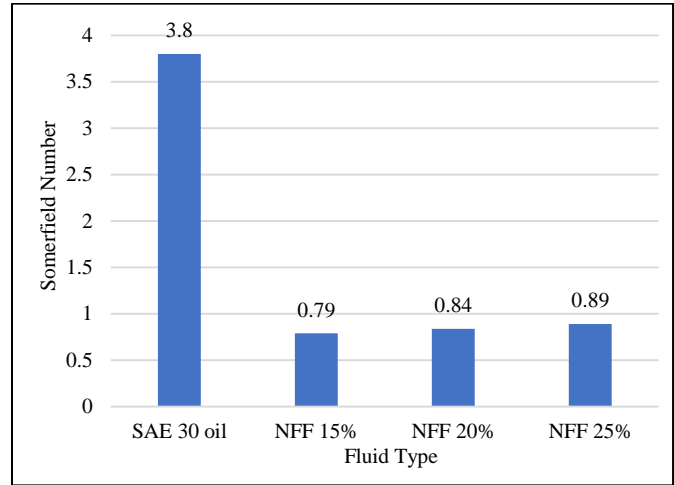


Fig. 10 Graphical representation of somerfield number for SAE 30 oil, nano ferro fluids 15 %, 20% and 25 % concentration oil

The graph describes the Somerfield number for SAE 30 oil is  $3.8 \times 10^6$ ; with the addition of nanoparticles of 15 % concentration, it is reduced to  $0.79 \times 10^6$ ; similarly, with the addition of 20% and 25% concentrations, it is reduced  $0.84 \times 10^6$  and  $0.98 \times 10^6$  respectively.

Table 10. Comparison of heat generated at maximum loads and speeds for SAE 30 oil and nano ferro fluid with different concertations

Type of Fluids	Heat Generated (Q <sub>g</sub> )
SAE 30 Oil	3.227
Nano Ferro Fluid with 15% Concertation	0.731
Nano Ferro Fluid with 20% Concertation	0.772
Nano Ferro Fluid with 25% Concertation	0.812

Table 10 offers a comparison of the Heat Generated (Q<sub>g</sub>) at maximum loads and speeds for different types of fluids: SAE 30 oil and nano ferrofluid with various concentrations. Heat generated values for SAE 30 oil is 3.227, which is lowered to 0.731 with the addition of 15% nanoparticles and 0.772 and 0.812 with the addition of 20% and 25% concentrations, respectively.

Using nano ferro fluids, heat-generated values are reduced compared to SAE 30 oil. The heat generated is a critical parameter as it indicates the amount of heat produced within

the bearing system during operation. The provided data demonstrates how different types of fluids and their concentrations can lead to varying levels of heat generation. Lower heat generation values for nano ferro fluids with different concentrations suggest that these fluids possess better lubricating and heat dissipation properties compared to SAE 30 oil. This information is important for assessing the bearing system's thermal performance and overall efficiency.

The graph describes the heat generated values for SAE 30 oil as 3.227; with the addition of nanoparticles of 15 % concentration, it is reduced to 0.731; similarly, with the addition of 20% and 25% concentrations, it is reduced to 0.772 and 0.81, respectively.

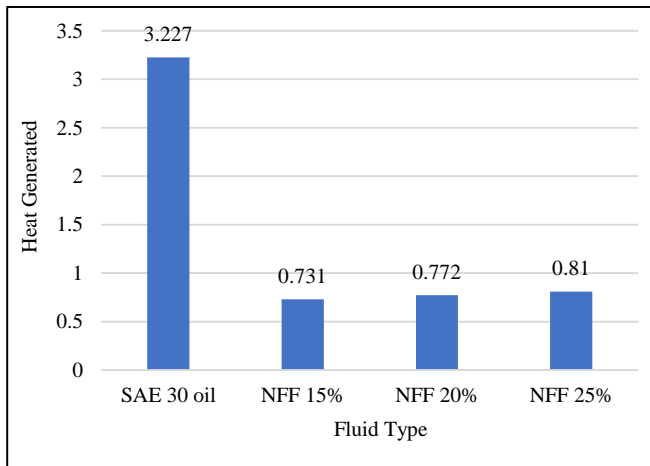


Fig. 11 Graphical representation of heat generated values for SAE 30 oil, nano ferro fluids 15 %, 20% and 25 % concentration oil

## 5. Conclusion

The experimental approach used two separate lubricants, namely SAE-30 oil and nano ferro fluids, in three different concentrations of 15%, 20%, and 25%, respectively, with three different suspended loads of 100 N, 150 N, and 200 N

## References

- [1] F. Quinci et al., "A Comparative Performance Assessment of a Hydrodynamic Journal Bearing Lubricated with Oil and Magnetorheological Fluid," *Tribology International*, vol. 162, 2021. [[CrossRef](#)] [[Google Scholar](#)] [[Publisher Link](#)]
- [2] K. P. Gertzos, P. G. Nikolakopoulos, and C. A. Papadopoulos, "CFD Analysis of Journal Bearing Hydrodynamic Lubrication by Bingham Lubricant," *Tribology International*, vol. 41, no. 12, pp. 1190-1204, 2018. [[CrossRef](#)] [[Google Scholar](#)] [[Publisher Link](#)]
- [3] Satish C. Sharma, and Nathi Ram, "Influence of Micropolar Lubricants on the Performance of Slot-Entry Hybrid Journal Bearing," *Tribology International*, vol. 44, no. 13, pp. 1852-1863, 2011. [[CrossRef](#)] [[Google Scholar](#)] [[Publisher Link](#)]
- [4] Robert Goraj, "Theoretical Study on a Novel Electromagnetically Supported Hydrodynamic Bearing under Static Loads," *Tribology International*, vol. 119, pp. 775-785, 2018. [[CrossRef](#)] [[Google Scholar](#)] [[Publisher Link](#)]
- [5] J. Bouyer, Y. Alexandre, and M. Fillon, "Experimental Investigation on the Influence of a Multi-Scratched Shaft on Hydrodynamic Journal Bearing Performance," *Tribology International*, vol. 153, 2021. [[CrossRef](#)] [[Google Scholar](#)] [[Publisher Link](#)]
- [6] Tushar P. Gundarameeya, and D. P. Vakharia, "Performance Analysis of Journal Bearing Operating on Nano Lubricants with TiO<sub>2</sub>, CuO and Al<sub>2</sub>O<sub>3</sub> Nanoparticles as Lubricant Additives," *Materials Today Proceedings*, vol. 45, no. 6, pp. 5624-5630, 2021. [[CrossRef](#)] [[Google Scholar](#)] [[Publisher Link](#)]

at three different rpms of 500, 600, and 700. A detailed tabular form is developed to compare each bearing design parameter.

The test results unequivocally demonstrate that the utilization of nano ferro fluids enhances essential bearing design parameters, including the bearing characteristic number, coefficient of friction, Sommerfeld number, and heat production. When we transition from regular fluids like SAE 30 oil to nano ferro fluids. When we modify the concentration of nano ferro fluids, such as 15%, 20%, and 25%, there is a minor fluctuation across the three distinct Nano ferro fluid concentrations. However, the improvement is considerable when compared to traditional fluids.

Finally, adding 15% Nano Ferro Fluid particles to base lubricating oil significantly influences and improves bearing design parameters such as bearing characteristic number, coefficient of friction, Somerfield number, and heat generation. The above information summarizes the experimental approach, findings, and conclusions from the research involving using different lubricants and concentrations in a bearing system. It effectively outlines the experimental setup, the comparison of results, and the benefits of using nano ferro fluids to enhance bearing design parameters. It showcases how changing the lubricant type and concentration can influence the performance and efficiency of the bearing system.

## Funding Statement

The Institute of Aeronautical Engineering supported this work.

## Acknowledgments

The authors would also like to thank the Institute of Aeronautical Engineering in Dundigal, Telangana, India, for providing experimental support and study facilities.

- [7] Z. Rasep, M. N. A. W. Muhammad Yazid, and S. Samion, "Lubrication of Textured Journal Bearing by using Vegetable Oil: A Review of Approaches, Challenges and Opportunities," *Renewable and Sustainable Energy Reviews*, vol. 146, 2021. [[CrossRef](#)] [[Google Scholar](#)] [[Publisher Link](#)]
- [8] Shasha Vali Shaik, D. Dev Singh, and Avinash Patil, "Experimental Investigation of Tribological Properties of TiO<sub>2</sub> Nanoparticles in Engine Oil," *Materials Today Proceedings*, vol. 46, pp. 883–889, 2021. [[CrossRef](#)] [[Google Scholar](#)] [[Publisher Link](#)]
- [9] Raman Kumar et al., "An Outline on Modern Day Applications of Solid Lubricants," *Materials Today Proceedings*, vol. 28, no. 5, pp. 1962-1967, 2020. [[CrossRef](#)] [[Google Scholar](#)] [[Publisher Link](#)]
- [10] Vineet Sharma et al., "Improvement in Frictional Behaviour of SAE 15W40 Lubricant with the Addition of Graphite Particles," *Materials Today Proceedings*, vol. 25, no. 4, pp. 719-723, 2020. [[CrossRef](#)] [[Google Scholar](#)] [[Publisher Link](#)]
- [11] Qin Dong et al., "Simulation and Experimental Verification of Fatigue Strength Evaluation of Journal Bearing Bush," *Engineering Failure Analysis*, vol. 109, 2020. [[CrossRef](#)] [[Google Scholar](#)] [[Publisher Link](#)]
- [12] Wenjie Zhou et al., "Research on the Lubricated Characteristics of Journal Bearing Based on Finite Element Method and Mixed Method," *Ain Shams Engineering Journal*, vol. 13, no. 4, 2022. [[CrossRef](#)] [[Google Scholar](#)] [[Publisher Link](#)]
- [13] Lubos Smolik et al., "Comprehensive Analysis of Fluid Film Instability in Journal Bearings with Mechanically Indented Textures," *Journal of Sound and Vibration*, vol. 546, 2023. [[CrossRef](#)] [[Google Scholar](#)] [[Publisher Link](#)]
- [14] Alexey V. KornaeV et al., "Enhanced Hydrodynamic Lubrication of Lightly Loaded Fluid-Film Bearings Due to the Viscosity Wedge Effect," *Tribology International*, vol. 160, 2021. [[CrossRef](#)] [[Google Scholar](#)] [[Publisher Link](#)]
- [15] Jongin Yang, M. M. Khonsari, and Alan Palazzolo, "CFD Investigation of Oil-Free Granular Lubrication," *Tribology International*, vol. 164, 2021. [[CrossRef](#)] [[Google Scholar](#)] [[Publisher Link](#)]
- [16] Bassam J. Alshaer, and Hamid M. Lankarani, "An Exact Analytical Solution for Dynamic Loads Generated by Lubricated Long Journal Bearings," *Mechanism and Machine Theory*, vol. 183, 2023. [[CrossRef](#)] [[Google Scholar](#)] [[Publisher Link](#)]
- [17] Zhongliang Xie, Jian Jiao, and Stanislaw Wrona, "The Fluid-Structure Interaction Lubrication Performances of a Novel Bearing: Experimental and Numerical Study," *Tribology International*, vol. 179, 2023. [[CrossRef](#)] [[Google Scholar](#)] [[Publisher Link](#)]
- [18] Shaoyu Zhu et al., "A Study of Misaligned Compliant Journal Bearings Lubricated by Non-Newtonian Fluid Considering Surface Roughness," *Tribology International*, vol. 179, 2023. [[CrossRef](#)] [[Google Scholar](#)] [[Publisher Link](#)]
- [19] P. Chellapandi, and C. Lakshmana Rao, "Development and Application of a Numerical Analysis Method for Investigating Hydro Static and Hydrodynamic Responses of Pocket Bearing Rotor Systems," *Journal of Fluids and Structures*, vol. 109, 2022. [[CrossRef](#)] [[Google Scholar](#)] [[Publisher Link](#)]
- [20] J. Bouyer, M. Wodtke, and M. Fillon, "Experimental Research on a Hydrodynamic Thrust Bearing with Hydrostatic Lift Pockets, Influence of Lubrication Modes on Bearing Performance," *Tribology International*, vol. 165, 2022. [[CrossRef](#)] [[Google Scholar](#)] [[Publisher Link](#)]
- [21] Nino Dakov, "Elastohydrodynamic Lubrication Analysis of a Radial Oil Seal with Hydrodynamic Features," *Tribology International*, vol. 173, 2022. [[CrossRef](#)] [[Google Scholar](#)] [[Publisher Link](#)]
- [22] Anil Singh, and Satish C. Sharma, "Behaviour of Conical Porous Hybrid Journal Bearing Operated with MHD Lubricant Considering Influence of Surface Irregularities," *Tribology International*, vol. 174, no. 6, pp. 107730-107736, 2022. [[CrossRef](#)] [[Google Scholar](#)] [[Publisher Link](#)]
- [23] Hussein Sayed, and T. A. El-Sayed, "A Novel Method to Evaluate the Journal Bearing Forces with Application to Flexible Rotor Model," *Tribology International*, vol. 173, no. 8, pp. 107593-107601, 2022. [[CrossRef](#)] [[Google Scholar](#)] [[Publisher Link](#)]
- [24] Long Zheng et al., "Numerical Simulation of Hydrodynamic Lubrication Performance for Continuous Groove-Textured Surface," *Tribology International*, vol. 167, 2022. [[CrossRef](#)] [[Google Scholar](#)] [[Publisher Link](#)]
- [25] Shengbo Li et al., "Active Hybrid Journal Bearings with Lubrication Control: Towards Machine Learning," *Tribology International*, vol. 175, 2022. [[CrossRef](#)] [[Google Scholar](#)] [[Publisher Link](#)]
- [26] Hussein Sayed, and T. A. El-Sayed, "Nonlinear Dynamics and Bifurcation Analysis of Journal Bearings Based on Second Order Stiffness and Damping Coefficients," *International Journal of Non-Linear Mechanics*, vol. 142, 2022. [[CrossRef](#)] [[Google Scholar](#)] [[Publisher Link](#)]
- [27] Atulkumar S. Patil, Vishnu D. Wakchaure, and Uddhav M. Shirsat, "Experimental Investigation of Micro-Textured Piston Ring and Cylinder Liner Pair at Mid Stroke Operating Conditions," *International Journal of Engineering Trends and Technology*, vol. 70, no. 10, pp. 381-392, 2022. [[CrossRef](#)] [[Publisher Link](#)]
- [28] Muhammad Imran Sadiq et al., "Investigation of Stiffness and Damping Coefficients in Fluid Film Bearing with Bio-Oils and Mineral-Based Oil," *Energy Reports*, vol. 8, pp. 419-429, 2022. [[CrossRef](#)] [[Google Scholar](#)] [[Publisher Link](#)]
- [29] Shaswat Saincher et al., "Experimental Investigation of Hydrodynamic Loading Induced by Regular, Steep Non-Breaking and Breaking Focused Waves on a Fixed and Moving Cylinder," *European Journal of Mechanics - B/Fluids*, vol. 93, pp. 42-64, 2022. [[CrossRef](#)] [[Google Scholar](#)] [[Publisher Link](#)]

- [30] N. S. C. Chaitanya, Y. V. V. Satyanarayana Murthy, and M. R. S. Satyanarayana, “Experimental Investigations on CI Engine for Performance, and Emissions Fuelled with Stabilised Binary Diesel/ JME Blends Doped with Nano Metallic Oxide Additive Particles using DEE, and Non- Ionic Surfactants,” *International Journal of Engineering Trends and Technology*, vol. 69, no. 8, pp. 161-173, 2021. [[CrossRef](#)] [[Publisher Link](#)]
- [31] Songlin Nie et al., “Failure Analysis of Auxiliary Support Bearing/Shaft Tribopair in Seawater Hydraulic Axial Piston Pump,” *Engineering Failure Analysis*, vol. 146, 2023. [[CrossRef](#)] [[Google Scholar](#)] [[Publisher Link](#)]
- [32] Huanhuan Wang et al., “Numerical Simulation on Hydrodynamic Lubrication Performance of Bionic Multi-Scale Composite Textures Inspired by Surface Patterns of Subcrenata and Clam Shells,” *Tribology International*, vol. 181, 2023. [[CrossRef](#)] [[Google Scholar](#)] [[Publisher Link](#)]